The Journal of Computer Science and Its Applications. An International Journal of the Nigeria Computer Society (NCS)
Vol. 29, No. 2, December, 2022

Comparative Evaluation of Image Segmentation Techniques for Flood Detection in High-Resolution Satellite Imagery

C. Agbo
Department of Computer Science, Federal University of Technology, Minna, Nigeria.
agbochristopher49@gmail.com

A. D. Mohammed
Department of Computer Science, Federal University of Technology, Minna, Nigeria.
drmalik@futminna.edu.ng

J. K. Alhassan
Department of Computer Science, Federal University of Technology, Minna, Nigeria.
jkalhassan@futminna.edu.ng

S. A. Adepoju
Department of Computer Science, Federal University of Technology, Minna, Nigeria.
solo.adepoju@futminna.edu.ng

Abstract— Speedy reaction to natural disasters, such as floods, is critical to minimising loss of life and pain. Access to fast and reliable data is critical for rescue teams. Satellite photography provides a wealth of data that may be analysed to assist pinpoint disaster-affected areas. The use of segmentation to analyse satellite images is becoming increasingly important in environmental and climatic monitoring, particularly in detecting and controlling natural disasters. Image segmentation improves pattern recognition, which divides a single image into several homogeneous pieces. The efficiency of image segmentation techniques varies depending on the layout of objects, illumination, shadow, and other variables. However, there is no one-size-fits-all method for successfully segmenting all imagery; specific methods are more efficient than others. This report compares four different technologies. Commonly used image segmentation techniques: K-means clustering (K.C.), Color thresholding (C.T.), Region-based Active Contour (R.A.C.) and Edge-based Active Contour (E.A.C.) segmentation. These four techniques were used to detect, and segment flooded areas in high-resolution satellite imagery. The K.C. method had the best flood segmentation rate with a Jaccard Index of 0.8234, Dice of 0.9234, the precision of 0.9589, recall of 0.9078 and BFscore of 0.9327, which was higher than the other three segmentation technique and previous works.

Keywords— Flood, High-resolution, Image segmentation, K-means Clustering, Satellite Imagery

1 Introduction

IMAGE Image segmentation is currently one of the essential jobs in image processing [1]. It has a wide range of applications, including clinical applications. satellite pictures, and others [2]. Several approaches for picture segmentation have been proposed and described. The most prevalent ways are edge detection-based segmentation, histogram-based method, Region-based segmentation, and Clustering-based segmentation. Remote sensing satellite images are critical to providing quantitative and qualitative geographic information [3]. Many scientific research and applications have benefited and enhanced because of the wealth of crucial insight generated by satellite images, depending on the desired studies, such as land surface mapping and monitoring, climate change investigation, ecology dynamics monitoring, urban planning, archaeological sites investigations, disaster monitoring, and global security [2], [4].

Satellite imaging has become a critical component in the planning of a variety of disciplines, including disaster management and the interpretation of natural disaster images [5]. When comparing the quantity, timeliness, and accessibility of satellite imagery covering a specific disaster incident today to the circumstance about ten years ago, has significantly improved [6]. It is critical to prioritise rescue missions, disaster response, and relief efforts following a disaster. These must be completed quickly and efficiently because resources are generally scarce in disaster-affected areas, and it is critical to pinpoint the places that have sustained the most damage [7]. Flooding is the most prevalent natural disaster, affecting people all over the world every year [8] In most situations, it directly impacts human life and causes property damage. Previous years have developed many approaches to better plan rescue operations in such scenarios [8] Flood mapping using satellite imagery is one area where a great deal of study has been done to monitor floods and do rapid risk assessments.

Image processing is a crucial step in mechanisms for visual perception, and It entails using computational models to retrieve relevant data from digital photographs [9]. Image segmentation is a technique for partitioning an image into different sections, which are generally dependent on the properties of its pixels, to interpret its content. Medical imaging, autonomous driving, and water management have all benefited from image segmentation

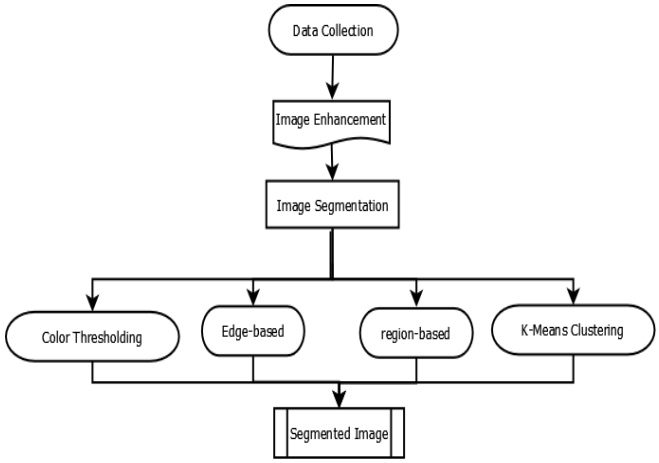

Fig. 1. Proposed System

[10]. Image segmentation may be used in flood disaster situations to separate the foreground from the backdrop. Researchers and industry employ a variety of image segmentation approaches, including thresholding, edge-based, region-based, and hybrid techniques [11]. Experiments from prior studies revealed that different picture segmentation approaches work better for various sorts of photos and situations. The goal of this research is to compare and contrast four picture segmentation algorithms., namely Region-based Active Contour (R.A.C.), Edge-based Active Contour (E.A.C.), K-means Clustering (K.C.), and Color Thresholding (C.T.) for flood detection on high satellite imagery. Hence, the significant contributions of this paper include:

1. Identification of flooded areas in high-resolution satellite imagery
2. Comparative experimentation of four different image segmentation techniques for flood detection.

The rest of the paper is laid out as follows: A synopsis of related research is presented in the second section. Section 3 explains the study's approach used to obtain the reported results. The experiment's findings and the conclusions obtained are discussed in Section 4. Finally, section 5 summarises the findings and considers potential future projects.

2 Related Works

Comparative analysis of six key segmentation techniques: clustering, edge-based, fuzzy logic, neural network, region-based and thresholding was presented by Jayapriya and Hemalatha [11]. The clustering technique was shown to have a long computing time in this investigation, whereas the edge-based was not suited for low-contrast images. The fuzzy logic technique's shortcoming was the difficulty in determining fuzzy membership. When segmenting overlapped grayscale pixel values, the region-based method was found challenging, while the thresholding technique was computationally expensive. This study recommended marker-based controlled watershed segmentation as a suitable method for medical image segmentation because it has minimal over-segmentation problems. However, this recommended marker-based controlled watershed segmentation technique suffers from an under-segmentation problem [12].

Prompted by the need to improve macroeconomic forecasts and shorten their time frames, Juergens and Meyer-Heß [13] concentrated on utilising very-high-resolution (V.H.R.) photographs to identify construction regions and their temporal variations in order to approximate construction spending as a driving force for economic forecasting. To discover construction zones and their temporal advancement, WorldView pictures from a location around the southern portion of Berlin, Germany, were subjected to multi-resolution segmentation accompanied by a K-Nearest Neighbor (K.N.N.) categorization. Construction zones have different material compositions than other land cover groups, resulting in distinct classification patterns. The V.H.R. picture suggests several sorts of sealed zones, like commercial or residential, may be distinguished. The identification of water, which is frequently classed as a sealed surface, is a significant problem for this paper. This is because there are only a few water samples in the scenarios.

A comprehensive evaluation of image segmentation strategies was presented by Abdulateef and Salman [14]. In this study, four segmentation strategies are discussed: threshold-based, edge-based, region-based, and energy-based segmentation. Each technique's benefits and drawbacks were discussed. It was discovered that no single technology can be considered best for all types of images, and that not all methods are suitable for each image type. However, no experimentation results were published in this work to illustrate how well any of the presented methods performed on image segmentation.

Ulmas and Liiv [4] employed a convolutional neural network (CNN) with an altered U-Net architecture to construct land cover categorization maps derived from satellite data. The study's purpose was to train and evaluate CNN models for autonomous land cover mapping and to see how effective they were in improving accuracy and detecting changes. The Big Earth Net satellite picture collection was used in this investigation. The built classification model had a high average F1 score of 0.749 on multiclass land cover classification with 43 probable picture labels. The algorithm also identifies noisy data in the Big Earth Net dataset, such as photos with inaccurate classifications. In addition, the model showed a high Mean Intersection Over Union (MioU) score ranging from 0.76 to 0.87 for land cover classes like woods, inland lakes, and arable land. The suggested model is not ideal for machine learning-based segmentation, as it has higher accuracy in some classes but lower results in visually less different classes.

Ye et al.[15] proposed a new remotely sensed edge detection technique that uses fast Guided filters to improve the image quality, then an upgraded Sobel operator with a 3 by 3 mask and eight directional templates to discover gradients and gradient orientations. A new two-dimensional Ostu approach was used to choose high and low thresholds. The PNG photographs of the University of the Chinese Academy of Sciences were utilised in the experiment. Although the suggested approach provides more edge details, crisp and continuous outlines, it has two drawbacks: high time complexity and inefficiency when dealing with high-intensity noise.

3 Methodology

This section presents the techniques used to achieve the aim of this study. Fig. 1 illustrates the methods used.

3.1 Dataset

Airbus Intelligence [16], NASA Earth Observatory [17] and Maxar Open Data Program (MODP) [18] were used to acquire data for this investigation. MODP is a rescue-in-action satellite imagery catalogue that is free and available to the public. The MODP was created to aid rescue missions in disaster management and emergency response. MODP gives brief descriptions and photographs of natural disasters such as hurricanes, tornados, wildfires, floods, explosions, and earthquakes. NASA's Earth Observatory houses satellite photos, stories, and findings of the environment, earth systems, and climate resulting from NASA research. Airbus Intelligence is a satellite imagery gathering, data processing, fusion, distribution, and intelligence collection expert. High-resolution SPOT satellite imagery is also included in the Airbus Intelligence. Figure 2 is an example of the Airbus Intelligence satellite imagery used in this study.

3.2 Image Enhancement

After collecting the RGB satellite imagery, the images were pre-

Fig. 2 Sample of Airbus Intelligence satellite imagery

processed using the Histogram Equalisation image enhancement technique. Image enhancement was performed at this stage because it highlights the more refined features in the colored satellite imagery andhe important information [3].

Compared to grey images, colour images contain more and richer information for visual perception. In Digital Picture Processing, colour image enhancement is critical. The pictures appear darker or with little contrast when the lighting is poor. Images with low contrast must be improved. The histogram equalisation approach is applied in this investigation. Histogram Equalisation is a technique for adjusting contrast in images by using the histogram [19]. The goal of this technique is to remap the scene's histogram to a distribution with a probability density function that is almost uniform.The equalisation of the histogram redistributes the intensity distribution. If an image's histogram has a lot of peaks and valleys, it will still have peaks and valleys after equalisation, but they will be moved. Histogram Equalisation is a technique for improving contrast and obtaining a homogeneous histogram [20] To conduct Histogram Equalization, the grayscale image's original histogram must be equalised. The cumulative histogram from the input image must be equalised to 255 by using (1) to create a new intensity value.

$$I(x) = \frac{d}{c_{max} - c_{min}} \times (C(x) - I_{min}) + I_0 \quad (1)$$

Where $I(x)$ is the new degree of intensity, d is the new value for dynamic range, I_0 is the new dynamic range's offset point for $I(x)$, $C(x)$ is the sum of the normalized values, c_{max} is the typical maximum value, and c_{min} is the normalised cumulative value's minimal value. Finally, cumulative histograms of the original image's mapping functions are normalised [20].

3.3 Image segmentation

The next step after performing the image enhancements is the image segmentation. Given that the image enhancements technique has highlighted the important information and more refined features, it is then appropriate to perform segmentation on the images. The enhanced images were segmented using four renowned techniques: Edge-based Active Contour (EAC), Region-based Active Contour (RAC), K-means Clustering (KC) and Color Thresholding (CT).

Image segmentation is typically a technique of disintegrating a digital photo into subgroups called Image segments in order to decrease the image's intricacy and facilitate subsequent alteration and evaluation.

3.3.1 Edge-based Active Contour (EAC)

Edge-based segmentation looks for inconsistencies in an image's intensity [21]. A border between two locations with significantly distinct attributes can be characterised as an edge. EAC is based on the idea that every picture sub-region is homogeneous enough that the transformation between them can be discerned only by discontinuity. EAC are closely tied to edge-based segmentation. Most EAC models have two parts: the regularity element, which determines the geometry of contours, and the boundary detection part, which draws the contour towards the borders [22]. Edge-based active contours may ignore the hazy borders because the picture gradient technique is used in both edge-based segmentation and EAC. For the image I(x, y), the edge functional is given in (2).

$$E_{edge} = -|\nabla I(x,y)|^2 \quad (2)$$

3.3.2 Region-based Active Contour (RAC)

Based on data collected from sub-regions, RAC approaches discover the ideal energy for which the model fits the image best. RAC models aim to discover each objects of interest by employing a specific region attribute to guide the movement of the active contour rather than the image gradient, and thus perform better for images with weak object boundaries [1]. Furthermore, RAC model is less affected by the position of original contours. A RAC can recognize inner boundaries regardless of the original contours' position.The usage of starting contours that have been pre-defined allows for independent segmentation [23]. RAC formula is as follows: Find the Contour C, which divides the picture into non-overlapping parts, given image I. (3) gives the model energy function.

$$F(c_1, c_2, C) = \lambda_1 \int_{inside(C)} |I(y) - c_1|^2 \, dy + \lambda_2 \int_{outside(C)} |I(y) - c_2|^2 \, dy + \mu|C| \quad (3)$$

Where μ is a constant, and C is any other variable curve, and inside(C) and outside(C) denote the regions inside and outside the contour C, correspondingly, and the constants c_1, c_2 dependent on C, is the average image intensity in inside C and correspondingly outside C. The first two entries on the right side of equation 3 provide global intensity information from I [24]. A diagram of the RAC technique used is shown in Figure 3.

3.3.3 Color Thresholding (CT) Image Segmentation

CT segmentation assumes that homogeneous colors in an image correlate to discrete clusters and consequently meaningful objects in the image, based on the color attribute of image pixels. To look at it differently, each group denotes a collection of pixels with the same color characteristics [25]. No single-colour space can deliver satisfactory results for all types of photos because segmentation results depend on the colour space employed [26]. This study uses

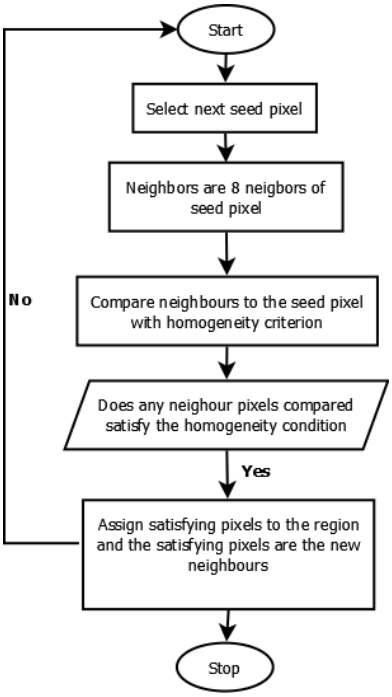

Figure3 RAC segmentation procedure

the Hue, Saturation, Value (HSV) colour space to segment colour images.

3.3.4 K-means Clustering (KC) Image Segmentation

Clustering is a method of grouping a collection of data into groups. One of the most widely utilized algorithms is KC. In KC, it divides a collection of data into a k number of data groups [27]. It separates a given collection of data into k unique clusters. There are two aspects to the KC algorithm. In the first phase, it identifies the k centroid, and then in the second stage, it shifts each point to the cluster with the nearest centroid to the data point [28]. The Euclidean distance is one of the most common ways for calculating the distance to the nearest centroid. It recalculates the new cluster centre, generates a new Euclidean distance between each centre and each data point depending on that centroid, and assigns the elements in the cluster with the least Euclidean distance after the clustering is complete. Separating the interest area from the background is also done using the unsupervised KC method [29]. Fig. 4 is a summary of the K-means segmentation procedure [30].

3.4 Performance Metric

1. Intersection-over-Union (IoU, Jaccard index): IoU also known as the Jaccard Index is a statistic for evaluating the accuracy of an object detector on a certain dataset. If the IoU prediction value is 1, the forecast is 100% right [31]. The lower the IoU, the less accurate the prediction. IoU is represented by (4):

$$\frac{\text{Area of Overlap}}{\text{Area of Union}} \quad (4)$$

2. Dice Similarity Coefficient (DSC): A DSC is a statistical tool that determines how similar two sets of data are. DSC is represented by (5).

$$DSC = \frac{2*\text{Area ofoverlap}}{\text{total number of pixels in both images}} \quad (5)$$

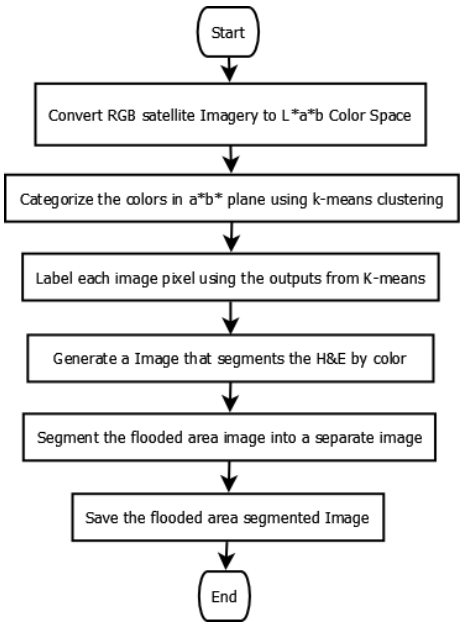

Figure 4 K-means segmentation procedure

3. Boundary F1 Score (BFS): The BF score is calculated by taking the harmonic mean (F1-measure) of the precision and recall values and adding a distance error tolerance to determine if a point on the predicted boundary matches the ground truth boundary. The BF score indicates how well an object's anticipated border fits the ground truth boundary. The formular for BFS is shown in (6)

$$\text{BFS} = \frac{2\times\text{precision}\times\text{recall}}{\text{recall} + \text{precision}} \quad (6)$$

4. Recall: The recall is calculated by dividing the number of sites on the ground truth boundary that are close enough to the predicted segmentation boundary by the length of the ground truth boundary. In other words, recall is the percentage of true positives discovered rather than missed.

$$Recall = \frac{TP}{TP+FN} \quad (7)$$

5. Precision: The ratio of the amount of pixels on the predicted segmentation's border that are near enough to the ground truth segmentation's boundary to the length of the predicted boundary is used to calculate precision. In other words, precision is the percentage of true positives versus false positives in a detection.. It is calculated using the formula in (6).

$$Precision = \frac{TP}{TP+FP} \quad (8)$$

Where TP is True Positives, TN is True Negatives, FN is False Negatives and Fp is False Positives. True positive is the pixel classified correctly as X, false positive is the pixel classified incorrectly as X; True Negative is the pixel classified correctly as not X, and false negative is the pixel classified incorrectly as not X.

3 Results and Discussion

In this study, experiments were conducted on four different image segmentation algorithms: Region-based active contour (RAC), Edge-based active contour (EAC), Color Thresholding (CT) and K-means Clustering (KC) concerning Flooded area identification and segmentation. The experiment was conducted on 24 satellite images. To avoid a cumbersome report, Table 1 shows the result obtained for six satellite images and the average performance of the four segmentation methods on these six images is also reported.

TABLE 1: EXPERIMENTAL RESULT FOR FLOOD DETECTION ON SIX SATELLITE IMAGES

Method	Images	Jaccard index	DSC	BFS	Precision	Recall
Region-based	Image1	0.5254	0.6889	0.5924	0.6427	0.5494
	Image2	0.5949	0.7460	0.5235	0.6813	0.4251
	Image3	0.6562	0.8148	0.6441	0.9055	0.4998
	Image4	0.5352	0.7065	0.6956	0.8196	0.6043
	Image5	0.4527	0.5215	0.6612	0.5986	0.7383
	Image6	0.6466	0.8068	0.8122	0.8755	0.7575
	Average	0.5685	0.7141	0.6548	0.7539	0.5956
Edge-based	Image1	0.3322	0.4770	0.3275	0.5900	0.2267
	Image2	0.3649	0.5189	0.3252	0.5945	0.2239
	Image3	0.3694	0.5245	0.5561	0.7180	0.4538
	Image4	0.4378	0.6050	0.4511	0.7985	0.3143
	Image5	0.3072	0.4432	0.3347	0.4022	0.2866

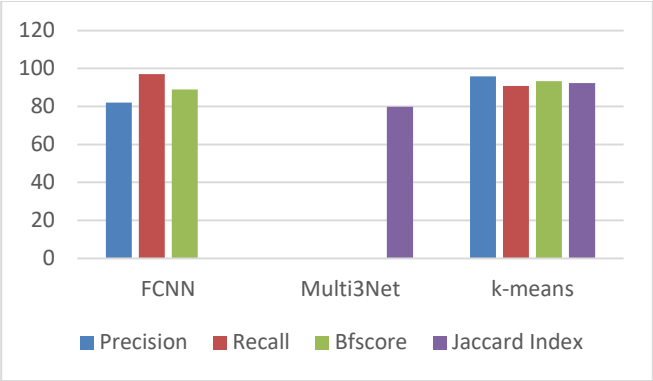

Figure. 5 Comparison of K-means clustering with related works

	Image6	0.4691	0.6316	0.4849	0.8979	0.3321
	Average	0.3801	0.5333	0.4133	0.6669	0.3062
Color image segmentation	Image1	0.6594	0.7948	0.9266	0.9046	0.9496
	Image2	0.6646	0.7985	0.9311	0.9047	0.9591
	Image3	0.7125	0.8785	0.8623	0.9892	0.7643
	Image4	0.8764	0.9313	0.9730	0.9977	0.9495
	Image5	0.8050	0.8539	0.8859	0.9190	0.8551
	Image6	0.6173	0.7888	0.8042	0.8863	0.7361
	Average	0.7225	0.8410	0.8972	0.9336	0.8690
K-means	Image1	0.7946	0.9457	0.9333	0.9504	0.9169
	Image2	0.6424	0.8143	0.9527	0.9647	0.9409
	Image3	0.7422	0.9032	0.8228	0.9890	0.7044
	Image4	0.9150	0.9539	0.9468	0.9787	0.9169
	Image5	0.7789	0.9333	0.8920	0.8991	0.8850
	Image6	0.8664	0.9498	0.9315	0.9304	0.9323
	Average	0.7899	0.9167	0.9132	0.9521	0.8827

Table 1 demonstrates that the K-means clustering method generated the best accuracy on the flooded area dataset, with an average Jaccard index of 0.7899, compared to 0.7225, 0.3801, and 0.5685, respectively, for CT, EAC, and RAC. With a DSC of 0.9167, the k-means clustering technique outperformed the CT technique, which had a DSC of 0.8410, and the RAC technique had a DSC of 0.7141. The EAC approach has the lowest DSC value of 0.5333, indicating that the ground truth and EAC segmentation are not very similar. However, 95.21% of the points detected by the k-means method were true positive predictions rather than false positives. Furthermore, CT detects a high percentage of actual positive predictions rather than false positives, with a precision of 0.9336. The EAC approach produced the least precision (0.6669), followed by the RAC technique (0.7539).

When the four approaches were compared using the BFScore performance metric, K-means clustering came out on top with a score of 0.9132, followed by CT with 0.8972, RAC with 0.6548, and EAC with 0.4133. Table 1 also reveals that K-means clustering has a high recall value of 0.8827, implying that the number of right positive predictions made out of all the positive predictions is better than CT, EAC, and RAC, which have recall values of 0.8690, 0.3062, and 0.5956, respectively.

After segmenting all 24 photos, K-means clustering achieved the best overall performance, with a Jaccard Index of 0.8234, a DSC of 0.9234, a precision of 0.9589, a recall of 0.9078, and a BFscore of 0.9327. The CT, which has a Jaccard index of 0.7456, DSC of 0.8690, the precision of 0.9465, recall of 0.8877, and BFscore of 0.9162, is the next method with good performance after k-means clustering. With a Jaccard index of 0.3957, DSC of 0.5555, the precision of 0.6578, recall of 0.3111, and BFscore of 0.4224, EAC performed the worst. On the 24 satellite pictures, RAC obtained an average Jaccard index of 0.5865, DSC of 0.7290, precision of 0.7783, recall of 0.6242, and BFscore of 0.6928. Table 2 shows a comparison of the best-performing method, k-means clustering, with previous works.

TABLE 2: COMPARISON OF K-MEANS CLUSTERING WITH RELATED WORKS

Method	Precision (%)	Recall (%)	BFscore (%)	Jaccard Index (%)
Fully convolutional neural network (FCNN) [32]	82	97	89	-
Multi3Net [33]	-	-	-	79.9
K-means clustering (proposed technique)	95.9	90.8	93.3	92.3

A comparison of the k-means clustering segmentation, Multi3Net, and FCNN is shown in Table 2. In comparison to Multi3Net and Fully convolutional neural networks, the suggested method achieved superior precision, recall, BFscore, and Jaccard index.

Fig 5 is a chart representing the performance of the proposed method in comparison with previous works as shown in Table 2. From the diagram it can be seen that only the Jaccard Index was used to measure the Multi3Net technique while theFCNN was measured using precision, recall and BFscore.

4 Conclusion and Future Works

This paper produced a comparative result for four image segmentation techniques: RAC, EAC, CT and KC, regarding flood detection on high-resolution satellite imagery. The obtained results demonstrate that different segmentation methods perform differently on satellite image segmentation. From the presented comparative analysis based on the Jaccard index, DSC, precision, BFscore, and recall performance metrics, the k-means clustering produced the best-segmented result with 0.8234 Jaccard Index, 0.9234 DSC, 0.9589 precision, 0.9078 recall and 0.9327 BFscore. This result shows the effectiveness of the k-means clustering segmentation technique in detecting flooded areas on high satellite imagery for effective flood detection. On the other hand, EAC obtained a low Jaccard index of 0.3957, DSC of 0.5555, the precision of 0.6578, recall of 0.3111 and BFscore of 0.4224. EAC's performance on high-resolution satellite photos demonstrates that it is not well adapted for flood detection. Based on the findings, it can be concluded that using the K-means clustering segmentation technique for flooded area identification delivers superior results to those found in previous studies. Finally, a comparison of four picture segmentation approaches for flood detection in high-resolution satellite images was provided.

The study made use of only four image segmentation techniques for flood identification on satellite imagery. For future work, the performance of more segmentation methods such as fuzzy logic and watershed segmentation methods on flood satellite images can be analysed. In addition, the performance of the four analysed techniques can be tested on other satellite imagery with different scenarios like vegetation, hurricanes, and buildings.

References

[1] [S. Soomro, A. Munir, and K. N. Choi, "Hybrid two-stage active contour method with region and edge information for intensity inhomogeneous image segmentation," PLoS ONE, vol. 13, no. 1, Jan. 2018, doi: 10.1371/journal.pone.0191827.

[2] P. Sathya and L. Malathi, "Classification and Segmentation in Satellite Imagery Using Back Propagation Algorithm of ANN and K-Means Algorithm," International Journal of Machine Learning and Computing, vol. 4, no. 1, pp. 422–426, 2011.

[3] I. Fawwaz, M. Zarlis, Suherman, and R. F. Rahmat, "The edge detection enhancement on satellite image using bilateral filter," in IOP Conference Series: Materials Science and Engineering, Feb. 2018, vol. 308, no. 1. doi: 10.1088/1757-899X/308/1/012052.

[4] P. Ulmas and I. Liiv, "Segmentation of Satellite Imagery using U-Net Models for Land Cover Classification," IEEE Access, vol. 4, Mar. 2020, [Online]. Available: http://arxiv.org/abs/2003.02899

[5] S. W. Park and Y. W. Lee, "Detection of forest disaster using high-resolution satellite images with semantic segmentation," Oct. 2019, p. 59. doi: 10.1117/12.2532990.

[6] S. N. K. B. Amit, S. Shiraishi, T. Inoshita, and Y. Aoki, "Analysis of satellite images for disaster detection," in International Geoscience and Remote Sensing Symposium (IGARSS), Nov. 2016, vol. 2016-November, pp. 5189–5192. doi: 10.1109/IGARSS.2016.7730352.

[7] K. Kaku, "Satellite remote sensing for disaster management support: A holistic and staged approach based on case studies in Sentinel Asia," International Journal of Disaster Risk Reduction, vol. 33. Elsevier Ltd, pp. 417–432, Feb. 01, 2019. doi: 10.1016/j.ijdrr.2018.09.015.

[8] N. A. Muhadi, A. F. Abdullah, S. K. Bejo, M. R. Mahadi, and A. Mijic, "Image segmentation methods for flood monitoring system," Water (Switzerland), vol. 12, no. 6, Jun. 2020, doi: 10.3390/w12061825.

[9] M. Geetha, M. Megha, A. S. Sarika, M. Mauktha, and R. N. Sethuraman, "Detection and Estimation of the Extent of Flood from Crowd Sourced Images," in International Conference on Communication and Signal Processing, 2017, pp. 603–608.

[10] P. Bhadoria, S. Agrawal, and R. Pandey, "Image segmentation techniques for remote sensing satellite images," in IOP Conference Series: Materials Science and Engineering, Dec. 2020, vol. 993, no. 1. doi: 10.1088/1757-899X/993/1/012050.

[11] P. Jayapriya and S. Hemalatha, "Comparative Analysis Of Image Segmentation Techniques And Its Algorithm," International Journal of Scientific & Technology Research, vol. 8, no. 10, pp. 2209–2212, 2019, Accessed: Apr. 15, 2022. [Online]. Available: www.ijstr.org

[12] M. Ogbuka. Kenneth, J. Agushaka, and I. O. Oyefolahan, "Overlapping Sickle Cells Detection and Separation using Marker-based watershed segmentation," i-manager's Journal on Image Processing, vol. 6, no. 4, p. 1, 2019, doi: 10.26634/jip.6.4.16752.

[13] C. Juergens and M. F. Meyer-Heß, "Identification of construction areas from vhr-satellite images for macroeconomic forecasts," Remote Sensing, vol. 13, no. 13, Jul. 2021, doi: 10.3390/rs13132618.

[14] Abdulateef and M. Salman, "A Comprehensive Review of Image Segmentation Techniques," Iraqi Journal for Electrical and Electronic Engineering, vol. 17, no. 2, pp. 166–175, Dec. 2021, doi: 10.37917/ijeee.17.2.18.

[15] H. Ye, M. Ding, and S. Yan, "Improved Edge Detection Algorithm of High-Resolution Remote Sensing Imagesbased on Fast Guided Filter," in IEEE 4th Information Technology and Mechatronics Engineering Conference, 2018, pp. 29–33.

[16] Airbus Intelligence, "Satellite Image Gallery | Airbus Intelligence," Satellite Image, 2021. https://www.intelligence-airbusds.com/newsroom/satellite-image-gallery/ (accessed Apr. 14, 2022).

[17] NASA, "NASA Earth Observatory - Home," Earth Observatory, 2021. https://earthobservatory.nasa.gov/ (accessed Apr. 14, 2022).

[18] Maxar, "High-resolution Satellite Imagery," Open Data Program, 2021. https://www.maxar.com/products/satellite-imagery (accessed Apr. 14, 2022).

[19] [19] R. Maini and H. Aggarwal, "A Comprehensive Review of Image Enhancement Techniques," vol. 2, no. 3, pp. 8–13, 2010.

[20] A. Kumar Vishwakarma and A. Mishra, "Color Image Enhancement Techniques: A Critical Review," Indian Journal of Computer Science and Engineering (IJCSE), vol. 3, no. 1, pp. 39–45, 2012.

[21] M. Ciecholewski, "An edge-based active contour model using an inflation/deflation force with a damping coefficient," Expert Systems with Applications, vol. 44, pp. 22–36, Feb. 2016, doi: 10.1016/j.eswa.2015.09.013.

[22] B. D. Baswaraj, A. Govardhan, P. Premchand, D. Baswaraj α, A. Govardhan σ, and P. Premchand ρ, "Active Contours and Image Segmentation: The Current State of the Art Active Contours and Image Segmentation The Current State of the Art Strictly as per the compliance and regulations of: Active Contours and Image Segmentation: The Current State of the Art," Type: Double Blind Peer Reviewed International Research Journal Publisher: Global Journals Inc, vol. 12, 2012.

[23] Q. O. Wong and Rajendran. Parvathy, "Image Segmentation using Modified Region-Based Active Contour Model," Journal of Engineering and Applied Sciences, vol. 14, no. 16, pp. 5710–5718, 2019.

[24] Y. Tian, M. Q. Zhou, Z. K. Wu, and X. C. Wang, "A region-based active contour model for image segmentation," in CIS 2009 - 2009 International Conference on Computational Intelligence and Security, 2009, vol. 1, pp. 376–380. doi: 10.1109/CIS.2009.238.

[25] D. Khattab, H. M. Ebied, A. S. Hussein, and M. F. Tolba, "Color image segmentation based on different color space models using automatic GrabCut," Scientific World Journal, vol. 2014, Aug. 2014, doi: 10.1155/2014/126025.

[26] R. Harrabi and E. ben Braiek, "Color image segmentation using multi-level thresholding approach and data fusion techniques: application in the breast cancer cells images," 2012. doi: 10.1186/1687-5281-2012-11.

[27] N. Dhanachandra, K. Manglem, and Y. J. Chanu, "Image Segmentation Using K-means Clustering Algorithm and Subtractive Clustering Algorithm," Procedia Computer Science, vol. 54, pp. 764–771, 2015, doi: 10.1016/J.PROCS.2015.06.090.

[28] N. Dhanachandra, K. Manglem, and Y. J. Chanu, "Image Segmentation Using K-means Clustering Algorithm and Subtractive Clustering Algorithm," in Procedia Computer Science, 2015, vol. 54, pp. 764–771. doi: 10.1016/j.procs.2015.06.090.

[29] D. Q. Zeebaree, D. Q. Zeebaree, H. Haron, A. Mohsin Abdulazeez, and S. R. M. Zeebaree, "Combination of K-means clustering with Genetic Algorithm: A review," International Journal of Applied Engineering Research, vol. 12, pp. 14238–14245, 2017, Accessed: Apr. 14, 2022. [Online]. Available: http://www.ripublication.com

[30] P. J. Baldevbhai and R. S. Anand, "Color Image Segmentation for Medical Images using L*a*b* Color Space," IOSR Journal of Electronics and Communication Engineering (IOSRJECE), vol. 1, no. 2, pp. 24–45, 2012, Accessed: Apr. 14, 2022. [Online]. Available: www.iosrjournals.orgwww.iosrjournals.org

[31] H. Rezatofighi, N. Tsoi, J. Gwak, A. Sadeghian, I. Reid, and S. Savarese, "Generalized Intersection over Union: A Metric and A Loss for Bounding Box Regression," Feb. 2019, [Online]. Available: http://arxiv.org/abs/1902.09630

[32] E. Nemni, J. Bullock, S. Belabbes, and L. Bromley, "Fully convolutional neural network for rapid flood segmentation in synthetic aperture radar imagery," Remote Sensing, vol. 12, no. 16, Aug. 2020, doi: 10.3390/RS12162532.

[33] T. G. J. Rudner et al., "Multi 3 Net: Segmenting Flooded Buildings via Fusion of Multiresolution, Multisensor, and Multitemporal Satellite Imagery," in The Thirty-Third AAAI Conference Artificial Intelligence (AAAI-19), 2019, pp. 702–709. [Online]. Available: www.aaai.org